Molecular-dynamics-simulation-guided membrane engineering of Saccharomyces cerevisiae by overexpression of plant FAE1 and GPAT5 genes increases fatty acid chain length in membrane lipids

Jeroen M Maertens
Chalmers University of Technology
Simone Scrima
The Danish Cancer Society Research Centre
Matteo Lambrughi
The Danish Cancer Society Research Centre
Samuel Genheden
Goteborgs Universitet
Cecilia Trivellin
Chalmers University of Technology
Leif A Eriksson
Goteborgs Universitet
Elena Papaleo
The Danish Cancer Society Research Centre
Lisbeth Olsson
Chalmers University of Technology
Maurizio Bettiga (maurizio.bettiga@chalmers.se)
Chalmers University of Technology https://orcid.org/0000-0001-5934-8720

Research

Keywords: lipidomics, membrane engineering, molecular dynamics simulations, robustness, Saccharomyces cerevisiae

Posted Date: March 17th, 2020

DOI: https://doi.org/10.21203/rs.3.rs-17482/v1

Molecular-dynamics-simulation-guided membrane engineering of *Saccharomyces cerevisiae* by overexpression of plant *FAE1* and *GPAT5* genes increases fatty acid chain length in membrane lipids

Jeroen M. Maertens[a]; Simone Scrima[b]; Matteo Lambrughi[b]; Samuel Genheden[c], Cecilia Trivellin[a]; Leif A. Eriksson[c]; Elena Papaleo[b]; Lisbeth Olsson[a]; Maurizio Bettiga*[a]

[a] Department of Biology and Biological Engineering, Division of Industrial Biotechnology, Chalmers University of Technology, Kemivägen 10, SE-412 96 Gothenburg, Sweden

[b] Computational Biology Laboratory, Danish Cancer Society Research Center, Strandboulevarden 49, 2100 Copenhagen, Denmark

[c] Department for Chemistry and Molecular Biology, University of Gothenburg, Medicinaregatan 9c 40530 Gothenburg, Sweden

Abstract

Background

The use of lignocellulosic-based fermentation media will be a necessary part of the transition to a circular bio-economy. These media contain many inhibitors to microbial growth, including acetic acid. Under industrially relevant conditions, acetic acid enters the cell predominantly through passive diffusion across the plasma membrane. The lipid composition of the membrane determines the rate of uptake of acetic acid, and thicker, more rigid membranes impede passive diffusion.

Results

We hypothesized that the elongation of glycerophospholipid fatty acids would lead to thicker and more rigid membranes, reducing the influx of acetic acid. Molecular dynamics simulations were used to predict the changes in membrane properties. Overexpression of *Arabidopsis thaliana* genes *FAE1* and *GPAT5* increased the average

*Corresponding author: Maurizio Bettiga; maurizio.bettiga@chalmers.se

fatty acid chain length. However, this did not lead to a reduction in the net uptake rate of acetic acid.

Conclusions

Despite successful strain engineering, the net uptake rate of acetic acid did not decrease. We suggest that changes in the relative abundance of certain membrane lipid headgroups could mitigate the effect of longer fatty acid chains, resulting in a higher net uptake rate of acetic acid.

Keywords: lipidomics; membrane engineering; molecular dynamics simulations; robustness; *Saccharomyces cerevisiae*

1. Background

The current linear model for resource utilisation and industrial production is unsustainable and must be shifted towards a more circular model. This means that bio-based processes will become increasingly important. Lignocellulosic biomass must be pre-treated and hydrolysed prior to being fermented to produce fuels, platform chemicals and other materials. Although pre-treatment and hydrolysis are essential to release sugars from the biomass, they also result fermentation medium containing many microbial growth inhibitors (1).

Acetic acid is a common inhibitor, and its concentration in pre-treated lignocellulosic sugar streams usually varies between 5 and 10 g/l (83-176 mM), although this depends on the raw material and type of pre-treatment (1). Acetic acid can be very damaging to *Saccharomyces cerevisiae* and even trigger apoptosis (2,3). At industrially relevant pH, acetic acid uptake occurs predominantly by passive diffusion of the undissociated acetic acid across the plasma membrane (PM) (Figure 1A) (4). Hence, acetic acid stress should be considered in terms of the concentration of the undissociated form, rather than the total concentration (pKa ~ 4.8). The intracellular pH of *S. cerevisiae* is generally higher than the pKa of acetic acid, causing the dissociation of acetic acid upon entering the cell (Figure 1A) (5). This in turn results in intracellular accumulation of anions and/or a reduction of intracellular pH (6,7). The ingress of undissociated acetic acid and its intracellular dissociation occurs until an equilibrium is reached between the intracellular and extracellular concentrations of undissociated acetic acid. It is therefore of the utmost importance to minimize the intracellular acetic acid concentration. This can be achieved by decreasing the ingress, increasing the efflux, or metabolising the acetic acid. Acetic acid is not usually metabolised by *S. cerevisiae* in the

presence of glucose (8), and efflux by active transport is energetically costly (9), and thus, this research focussed on reducing the ingress.

The PM of *S. cerevisiae* is composed of lipids, sterols and membrane proteins. The main protein in the PM is Pma1 (10), and the main sterol is ergosterol (ERG). The latter can reside partly in the interior of the lipid bilayer, increasing membrane rigidity (11). The lipid fraction of the *S. cerevisiae* PM consists of several of lipids, and a simplified schematic of *S. cerevisiae* lipid metabolism is shown in Figure 1B. More comprehensive descriptions of *S. cerevisiae* lipid metabolism have been published previously (12,13). *De novo* fatty acid (FA) synthesis in *S. cerevisiae* is catalysed by a complex consisting of Fas1 and Fas2. This complex produces acyl chains with lengths of up to eighteen carbon atoms (C18). Elongation of FAs up to C24 is performed by Elo2, while Elo3 is responsible for the elongation of FAs up to C26. The C26 FAs produced by Elo3 are typically used for sphingolipid production. The sphingolipids consist of ceramides (Cer), which are toxic (14), and complex sphingolipids, i.e., inositol phosphorylceramide (IPC), mannosyl-inositol phosphorylceramide (MIPC) and mannosyl-di-(inositol phosphoryl) ceramide ($M(IP)_2C$) (Figure 1B).

The glycerophospholipids (GPLs) are the main group of membrane lipids, and their important components are included in Figure 1B. GPL headgroups with one, rather than two, acyl chains are called lyso-glycerophospholipids (L-GPLs) and are conically shaped due to the large headgroup and small tail end (Figure 1A). Other membrane lipids also have characteristic shapes: sphingolipids, phosphatidylcholine (PC), phosphatidylserine (PS) and phosphatidylinositol (PI) are considered cylindrical, while phosphatidic acid (PA), phosphatidylethanolamine (PE) and diacylglycerol (DAG) are considered conical with a small headgroup (Figure 1A). The shape can affect the membrane structure and, in addition to the

84 different membrane components and their headgroups, FA chain length and degree of
85 saturation are important factors affecting membrane properties such as the area per lipid
86 (APL) and the rigidity of the membrane (15).

87 Research on the modification of the membrane composition of organisms has recently been
88 summarized in a review by Qi et al. (16). While membrane engineering research focusses
89 mainly on bacteria, there is growing interest in altering the membrane composition of
90 yeasts. The first papers on this subject, on the model organism *S. cerevisiae*, have already
91 been published (17). However, the components of plasma membranes are part of complex
92 and highly regulated metabolic systems, and not all membrane engineering research has
93 been unequivocally successful (18).

94 The properties of the PM determine the rate of uptake of acetic acid as it enters the cell
95 through passive diffusion. Generally, thicker and more rigid membranes impede passive
96 diffusion (19), and we therefore propose membrane engineering as a tool to achieve these
97 properties to reduce acetic acid uptake in *S. cerevisiae*. Specifically, we propose the
98 engineering of *S. cerevisiae* to incorporate longer acyl chains into GPLs. In *S. cerevisiae*, very-
99 long-chain FAs are almost exclusively used in the production of storage lipids and
100 sphingolipids, although *S. cerevisiae* can incorporate very-long-chain FAs into GPLs when
101 sphingolipid production is suppressed. Plant FA elongases are not affected by *S. cerevisiae*
102 lipid elongation control systems (20), and are thus the most suitable candidates to increase
103 the relative abundance of very-long-chain FAs in *S. cerevisiae*. Plants have several different
104 FA elongases, and some *Arabidopsis thaliana* elongases have previously been expressed in
105 *S. cerevisiae*, each producing a specific FA profile (20). With respect to the goal of elongating
106 yeast membrane lipids, FAE1 (KCS18) was identified as the most interesting due to its role in

the production of FAs with chain lengths of up to C26 (Figure 1B). Once produced, the FAs can be incorporated into phospholipid biosynthesis, a function performed by glycerol-3-phosphate acyl transferase (GPAT). Plants have a range of GPAT enzymes and each enzyme may have a preference for specific FAs (21). *A. thaliana* GPAT5 has a preference for FAs with chain lengths compatible with FAE1 production (21). Therefore, the engineering strategy used to incorporate longer-chain FAs into *S. cerevisiae* GPLs was to overexpress the *A. thaliana* genes *FAE1* and *GPAT5* under strong promotors via integration of the recombinant constructs in the *S. cerevisiae* genome (Figure 1B).

In order to predict which changes in membrane composition could have the most relevant effect on membrane rigidity and permeability, we modelled the expected outcome of our engineering strategy using Molecular dynamics (MD) simulations. Shotgun lipidomics were employed for lipidomic profiling of all strains produced in this study and the data was used to analyse membrane composition and provide valuable information and insight into the effects of this engineering approach. Finally, we investigated whether changes in the membrane affected the intracellular concentrations of acetic acid over time.

2. Results and discussion

2.1. Long-chain glycerophospholipids increase the rigidity of *in silico* membranes in a concentration-dependent manner.

MD simulations were used to investigate how increasing the concentrations of long-chain FA GPLs affect the structural properties of yeast membrane models. PM permeability in *S. cerevisiae* is dependent on its lipid composition (4,22). In particular, lipids with long- and very-long-chain FAs determine membrane rigidity by increasing the membrane thickness and lipid packing (23). Long-chain GPLs were introduced into *in silico* models of yeast membranes whose structural properties have been investigated previously (4,22). Starting

from the reference systems, i.e. Null-64 and Null-256, eight different bilayer membrane were constructed, each having a specific lipid composition (Table 1). The number of sterol and sphingolipid molecules (i.e. ERG and IPC) was constant in all the systems. The lipids of the PC and PI classes in the reference system (i.e. DOPC (1,2-dioleoyl-*sn*-glycerol-3-phosphocholine) and POPI (1-palmitoyl-2-oleoyl-*sn*-glycerol-3-phospho-(1'-myoinositol)) were replaced with long-chain GPLs with increasing relative abundances (8, 16, 24, 32, 40, 48, 64 and 96%) (Table 1), rising the average GPL chain length by 0.017 carbon atoms/$\%_{increase}$ (e.g. 24 % x 0.017 carbon atoms/$\%_{increase}$ = 0.41 increase in carbon atoms compared to the Null systems). More specifically, the GPLs used contain acyl chain lengths of 20 (AOPC (1-arachidoyl-2-oleoyl-sn-glycero-3-phosphocholine)/AOPI (1-arachidoyl-2-oleoyl-sn-glycero-3-phospho-*(1'-myo-inositol)*)), 22 (BOPC (1-behenoyl-2-oleoyl-sn-glycero-3-phosphocholine)/BOPI (1-behenoyl-2-oleoyl-sn-glycero-3-phospho-*(1'-myo-inositol)*)) and 24 (LOPC (1-lignoceroyl-2-oleoyl-sn-glycero-3-phosphocholine)/LOPI (1-lignoceroyl-2-oleoyl-sn-glycero-3-phospho-*(1'-myo-inositol)*)) carbons at the *sn1* position, based on the expected fatty acid production profile of FAE1 (20). These ten membrane systems were used as starting points to perform multi-replicate 200-500 ns unbiased MD simulations using a modified version of Stockholm lipids force field (Slipids ff) (22) (Table 1). The MD ensembles were studied by calculating three parameters: i) the APL ii) the membrane thickness (MT) and iii) the deuterium order parameter (S_{CD}) of the *sn1* acyl chains of POPI and DOPC (Figure 2, Additional file 1-S3).

A clear trend was observed in the MD simulations, showing that long-chain GPLs affected the structural properties of the membrane in a concentration-dependent manner (Figure 2). Increasing concentrations of long-chain lipids resulted in denser (lower APL), thicker (larger MT) and more rigid (higher S_{CD}) membranes. The increasing number of long-chain GPLs rises

155 the attractive van der Waals forces between acyl chains, leading to an increase in the
156 packing density of the lipid molecules in the membrane, and a gradual decrease in APL
157 (from 0.541 ± 0.004 to 0.503 nm^2 ± 0.008 at 96%) (Figure 2A). The greater proportion of long
158 acyl chains in the tightly packed membrane increases the MT (from 4.325 ± to 4.808 nm ±
159 0.079 at 96%) (Figure 2B). S_{CD} exhibited a less clear behaviour, and a substantial increase
160 was seen only at 96%; the trend being similar for both the DOPC and POPI *sn*1 acyl chain
161 (Figure 2C and D). Overall, the results of the MD simulations suggest that long-chain GPLs
162 reshape the membrane towards more rigid and more densely packed states in a
163 concentration-dependent manner, thereby reducing their fluidity, which is important in
164 determining their permeability to small molecules such as acetic acid (24). In addition to
165 these results, it has previously been shown that the GPLs and sphingolipids in the acetic-
166 acid-tolerant *Zygosaccharomyces bailii* not only have longer acyl chains, but this strain is
167 also able to increase the average length of its membrane lipids under acetic acid stress by
168 increasing the relative abundance of sphingolipids (25). The results of our simulations and
169 the above findings thus indicate that elongating the GPL acyl chain length could reduce
170 acetic acid uptake.

171 **2.2. Overexpression of *FAE1* and *GPAT5* results in an increase in lipid chain length**

172 Synthetic, codon-optimised versions of *FAE1* and *GPAT5* (Additional File 1-S1) were inserted
173 into expression vectors using modular cloning for *S. cerevisiae* (26). Introduction of the *FAE1*
174 and *GPAT5*-containing plasmids into *S. cerevisiae* resulted in two single-gene expression
175 transformants containing a plasmid, and one double transformant with *FAE1* and *GPAT5*
176 integrated into the genome (FAE1_GPAT5) (plasmid maps: Additional file 1-S2). Initial
177 characterisation of the single and double transformants revealed high clonal variation for

178 the single transformants. In addition, the *GPAT5* single transformants showed significantly
179 reduced growth and inconsistent specific growth rate, even when working with a specific
180 clone. It is known that 2-micron-based gene expression can lead to high variation in both
181 plasmid and gene copies (26). Therefore, experimental findings regarding the single
182 transformants will not be further discussed in this paper. However, information is available
183 in the supplementary material (Additional File 1-S4,S6, Additional file 2). No significant
184 differences were seen in the growth characteristics of the double transformant and those of
185 the empty plasmid control (EPC); not in the growth profiler set-up (Additional file 1-S7), nor
186 in aerobic shake flask experiments using defined buffered medium (pH 5).

187 Fatty acid methyl esterification and gas chromatography analysis of total lipids revealed that
188 15% (±1) of the total lipids in the FAE1_GPAT5 strain had chain lengths of C20-24, while the
189 EPC contained only 0.20% (±0.07) total lipids with these chain lengths (Additional file 1-S8).
190 Thus, the engineering strategy was successful in increasing the length of FAs in the total
191 lipids in *S. cerevisiae*.

192 **2.3. Shotgun lipidomics confirmed successful strain engineering and revealed a shift in**
193 **lipid profiles towards increased acyl chain length and more conically shaped lipids**

194 To analyse the impact of the metabolic engineering strategy on the PM more precisely,
195 shotgun lipidomics were performed in triplicate on a representative transformant of each of
196 the different strains. In order to obtain as complete data as possible, total cell extracts were
197 used for lipidomics and analysis included all common lipid metabolites and intermediates,
198 including sphingolipids. The analysis also included ergosterol esters (EEs), although free
199 esters (i.e. ERG) could not be included. The raw lipid data is available in the supplementary
200 material (Additional file 2).

The shotgun lipidomics detected a total of 277 and 534 separate metabolites for the EPC and FAE1_GPAT5 strain, respectively. The EPC exhibited the highest relative abundance of unsaturated lipids, both in total lipids (88.7% (σ=0.5)) unsaturated in the EPC versus 85.0% (σ=1.0) in the FAE1_GPAT5) and in the membrane-related lipids, where the EPC contained 85.1% (σ=0.7) unsaturated lipids, and the double transformant 80.4% (σ=1.2). Thus, the double transformant strain had relatively more saturated lipids than the control strain, which is known to increase membrane order (27).

As our primary interest was the PM, phosphatidylglycerol (PG) and cardiolipin (CL) were considered separately, as they are only present in mitochondrial membranes. The FAE1_GPAT5 strain had a significantly higher proportion of FAs residing in the PM than the EPC: 71.0% (σ=1.0) versus 68.0% (σ=0.5), respectively. The relative abundances of FA chains in different lipid groups are summarised in the supplementary material (Additional file 1-S4).

2.3.1. Glycerophospholipids and sphingolipids

The goal of strain engineering in this study was to create thicker, more rigid membranes by elongation of the glycerophospholipids' fatty acids. Hence, the main goal of the lipidomics was to confirm that the chain elongation revealed in the total lipid screening persisted in PM lipids, including the sphingolipids, as they play a major role in membrane thickness and rigidity, and are thus also of the greatest interest.

A simplified method of comparing complex lipid chain length data is to compare average chain lengths over all the membrane lipids of different strains, and this is also a suitable way of comparing wet-lab results to the MD simulations. It was found that the FAE1_GPAT5 transformant exhibited a clear increase in the average number of carbons per GLP molecule compared to the EPC. More specifically, the FAE1_GPAT5 strain had, on average, 34.00

(σ=0.02) carbons in the FA chains of a single GPL molecule, while the value for the EPC was only 33.57 (σ=0.014) carbons per GPL molecule. This means that engineering increased the average chain length by about 0.43 carbons per GPL molecule. The MD simulations predicted relatively longer carbons on average (34 for Null-256), but the average increase in chain length was comparable to that in the MD system containing 24% long-chain GPLs (0.017 x 24 = 0.41 increase in carbon chain length). When comparing this MD model to the Null-256 model, the APL could be expected to decrease from 0.541 nm^2 (σ=0.004) to 0.525 nm^2 (σ=0.005). Additionally, the MT would have increased from 4.325 nm (σ=0.04) in the Null-256 model to 4.465 nm (σ=0.014) in the 24% long-chain GPL model.

The long glycerophospholipids were clearly more abundant in the FAE1_GPAT5 strain than in the EPC (Figure 3A), as the fraction of GPL that had <36 carbons in both fatty acid chains combined was 13.22% (σ=0.17), while it was only 0.200% (σ=0.009) in the EPC.

In addition to changes in the chain length, changes were also observed in the headgroups (Figure 3B). The cylindrical membrane lipids (PC, PS, PI and sphingolipids) were the most abundant in both strains, however, they were slightly less abundant in FAE1_GPAT5 (66.5%, σ=0.6) than in the EPC (67.9% σ=0.4). Conically shaped membrane lipids are found in two groups: the first being lipids with only one fatty acid chain, where the head is the largest part of the molecule (L-GPL), and the second being lipids with two fatty acid chains, where the headgroup is the smallest part of the molecule (DAG, PA, PE) (Figure 1A). Lipids with a small headgroup constituted 31.3% (σ=0.5) of membrane lipids in the FAE1_GPAT5 strain, which was significantly higher than in the EPC strain (28.99%, σ=0.18). The most conically shaped membrane lipids, DAGs, were particularly more abundant when *GPAT5* was

overexpressed: 12.34% (σ=0.16) in the FAE1_GPAT5 strain, while this was only 7.0% (σ=0.6) in the EPC (Figure 3B).

The GPL lipids PS and PI were significantly reduced in the FAE1_GPAT5 strain, compared to the EPC (Figure 3B). These GPLs are conically shaped (small head), positively charged, and enriched in the inner membrane leaflet. The proportions of conically shaped lipids that enrich in the outer leaflet (sphingolipids and PC) did not differ significantly between the two strains (Figure 3B).

Many membrane lipids and have specific traits, such as charge or conformation, and are often arranged asymmetrically between the two membrane leaflets. Therefore, it is difficult to predict how the many changes in headgroup composition between the EPC and the FAE1_GPAT5 strain will affect the PM properties on the cellular level.

2.3.2. Storage lipids

The storage lipids analysed were of two groups: the triacylglycerols (TAGs) and the EEs (Figure 1B). In the FAE1_GPAT5 strain, more long-chain FAs were incorporated in both TAGs and EEs than in the EPC. In the EPC, the TAGs generally had acyl chains of 50 or 52 carbons in total (67.1%, σ=0.5), while only 9.6% (σ=0.5) of the TAG total FA chain length was C53-60. The FAE1_GPAT5 strain, in contrast, had longer-chain FAs (C53-60) in 31.8% (σ=0.8) of the TAGs, while only 39.6% (σ=1.1) of TAG total FA chain length was C50-52. The EEs of the EPC consisted of 99.1% (σ=0.2) ergosterol bound to an acyl chain of either C16 or C18, and no EEs with longer FA chains were detected. However, in the FAE1_GPAT5 strain, 3.57% (σ=0.05) of the EEs were bound to chains longer than C18. Finally, FAE1_GPAT5 exhibited a reduced relative abundance of EEs.

2.4. The maximum intracellular acetic acid concentration in the FAE1_GPAT5 strain was reduced, although the uptake rate was higher

As the metabolic engineering strategy was successful in terms of elongating the FAs in membrane lipids, the acetic acid uptake rates of the strains were evaluated. The uptake of acetic acid over time was investigated at four different concentrations of acetic acid (0.56, 2.4, 20 and 144 mM) with a constant buffered pH of 5.0. The FAE1_GPAT5 strain showed lower maximum intracellular acetic acid concentrations than the EPC strain at all concentrations investigated (90% confidence level) (Figure 4, Additional file 1-S5). Incubation at the high, industrially relevant concentration of 144 mM extracellular acetic acid, caused the EPC to rapidly reach a similar intracellular concentration of acetic acid, indicating that the intracellular pH was reduced to 5, as can be seen in Figure 4. However, the average maximum intracellular concentration of acetic acid in the FAE1_GPAT5 strain was 96.6 mM, which indicates an intracellular pH of 4.7, calculated using the Henderson-Hasselbalch equation. Using the same method to calculate the intracellular pH at low, non-stressing concentrations of acetic acid (0.56 and 2.4 mM), showed that the FAE1_GPAT5 strain had an intracellular pH of 6.0, while the intracellular pH of EPC was 6.1.

In order to confirm that the ingress of acetic acid into the cells occurred predominantly by passive diffusion, kinetic experiments were performed on the FAE1_GPAT5 strain and the EPC. The results presented in Figure 5 show a strong linear correlation ($R^2 \leq 0.99$) between sampling points of the same strain, confirming that the passive uptake of acetic acid is the main method of ingress into the cell. In addition to the linearity of the correlation, the slope can be used to indicate the net uptake rate of acetic acid. The linear regression line for the FAE1_GPAT5 had a slope of 0.153, while that for the EPC was 0.118, indicating that the net ingress of acetic acid into the FAE1_GPAT5 cells was higher than in the EPC. This was an

unexpected result considering that the initial aim of increasing the FA chain length in the membrane was successful, and should have resulted in the membrane being thicker and more rigid, which was hypothesised to reduce passive uptake. However, the lipidomics showed that, besides longer-chain fatty acids being included in all lipid groups, the headgroups of the GPLs drastically changed. In particular, the FAE1_GPAT5 strain contained significantly higher relative amounts of conically shaped DAGs (Figure 3B). Previously published results of membrane simulations show that high levels of DAGs are able to break the lamellar structure of the plasma membrane, reducing its integrity (28). Other research has shown that DAGs can be highly localised in specific areas of the membrane during cellular growth (29), potentially increasing the damage to the lamellar structure of the membrane. However, low concentrations of DAGs can replace ERG in membrane microdomains (30), making the membrane more rigid (11). Besides the membrane structure itself, it is possible that transformants have a different rate of acetic acid efflux, which could influence the net influx of acetic acid.

3. Conclusions

The results of the MD simulations indicated that long-chain GPLs alter the plasma membrane towards more rigid and packed states in a concentration-dependent manner. Strain engineering was successful in increasing the average FA chain length in all membrane and storage lipids. Despite this, the FAE1_GPAT5 double transformant seemed to have an increased rate of net acetic acid uptake and reduced ability to maintain pH homeostasis compared with the background strain. We suggest that changes in the relative abundance of certain membrane lipid headgroups (e.g. DAG lipids) could mitigate the effect of longer fatty acid chains, resulting in a higher net uptake rate of acetic acid.

4. Methods

4.1. Molecular dynamic simulations

4.1.1. Membrane modelling and simulation set-up

Eight models of lipid membranes with increasing concentrations of different types of long-chain GPLs (indicated as M1-M8, see Table 1) were constructed based on previously published yeast membrane models (4,22). Multi-replicate unbiased MD simulations were performed for ten systems (Table 1). *Gromacs v5.1* (31) was used together with a modified version of the Slipids ff (32–34) in which the topologies and parameters for additional lipids have been included as explained in the original article (22). Each of the ten system was solvated in a rectangular box of water molecules (40 water molecules for each lipid in the membrane) using the TIP3P model (35). The net charge was neutralized by adding 32-128 sodium ions depending on the system. The same approach was used for the solvation and charge neutralization of all the membrane systems described below. A membrane system composed of 64 lipid molecules was produced with the CHARMM Membrane Builder (36). The lipid composition of the membrane was: 22 molecules of DOPC as representatives of the PC class, 32 molecules of POPI as representatives of the PI class, and ten molecules of ERG as representatives of the sterols. The resulting system was minimized using a 1000-step steepest-descent algorithm. After minimization, ten random POPI molecules were replaced by ten IPC molecules using an *in-house* Python script (obtaining a system denoted Null-64 in Table 1). A 1000-step minimization was performed followed by an equilibration step of 5 ns in the NPT ensemble with a 4-fs time step. The membrane systems described below followed the same protocol. The equilibrated 64-lipid membrane was then expanded along the x and y dimensions, producing a system composed of 256 lipids. We used this system (denoted Null-256 in Table 1) as the starting point for our study to introduce the long-chain

GPLs: AOPC and AOPI with the *sn1* acyl chain length of 20 carbons, BOPC and BOPI with the *sn1* acyl chain length of 22 carbons, LOPC, and LOPI with the *sn1* acyl chain length of 24 carbons (Table 1). The AOPC/AOPI, BOPC/BOPI and LOPC/LOPI were added at a ratio of 4:2:1, with total contents of long-chain GPLs of 8, 16, 24, 32, 40, 48, 64 and 96% (Table 1). These percentages were calculated as the content of long-chain GPLs divided by the total amount of GPLs (i.e., DOPC, POPI and long-chain lipids). The Slipids ff topologies of the long-chain GPLs AOPC, BOPC, LOPC and AOPI, BOPI, LOPI were obtained by adapting the topologies of the 1-stearoyl-2-oleoyl-sn-glycero-3-phosphocholine and of the POPI, respectively. This adapting step was performed using *in-house* Python scripts. The *sn1* chains of random DOPC and POPI molecules of the Null-256 system were elongated and saturated. All covalent bonds were constrained with the LINCS algorithm (37), and periodic boundary conditions were employed for the preparation steps and the productive MD simulations. The Parrinello-Rahman barostat (38) was used with a 10-ps coupling constant, while the temperature was kept at 298 K using the Nosé-Hoover thermostat (39) with a 0.5 ps time constant. The particle-mesh Ewald switch summation method was employed to treat electrostatic interactions (40). Switch cut-offs of 1.2 nm were used for Van der Waals and short-range Coulomb interactions. Three to five replicates of unbiased MD simulations were performed for each of the ten systems, each being of 200-500 ns of length (Table 1). An *in-house* Python script was used to implement the hydrogen mass repartitioning approach (41) to remove the fastest degrees of freedom in the system, allowing the use of time steps up to 4 fs in the MD simulations. The hydrogen mass was increased by a factor of four, from 1.008 u to 4.0320 u. This approach has been tested in simulations of a variety of membranes, showing practically no differences in their structural properties when compared to non-heavy hydrogen simulations (41). At least three independent replicates

were collected for each system (Table 1), using different initial random seeds for the simulation (42,43).

4.1.2. Analysis of the membrane properties

The output of the MD simulations provided three structural parameters commonly used to study membranes and to validate simulation ensembles against experimental data (44): i) the APL, ii) the MT and iii) the S_{CD}. All the analyses were carried out using *in-house* Python scripts.

The APL was calculated as the lateral area of the membrane divided by the total number of lipids in one leaflet:

$$APL = \langle L_x L_y / N \rangle \quad (1)$$

where, *Lx* and *L*y are the lateral dimensions of the membrane, and *N* is the total number of lipids in one leaflet. The angular brackets denote the ensemble average. The average bilayer thickness was calculated as the average distance between the phosphate groups of the lipid heads in two opposing leaflets of the membrane. S_{CD} was calculated as a measure of the carbon bond rigidity of the acyl chains in the lipids in the membrane, according to:

$$S_{CD} = \langle [3cos^2 \theta_{(t)} - 1\,]/2 \rangle \quad (2)$$

where θ describes the orientation of the carbon–hydrogen bond vector with respect to the membrane-normal vector at time t. S_{CD} was calculated for all the carbon atoms in the *sn1* acyl chains of POPI and DOPC. The three structural parameters were computed for each of the four 200 ns replicates of the Null-256 system and each of the three to five 300 ns replicates of the longer-chain membrane systems. Mean values averaged over the number of simulation frames and standard deviations of the structural parameters were calculated (Additional file 1: Figure S5). The means and standard deviations of the three structural

parameters were calculated for three replicates of each membrane system to provide MD ensembles with comparable sizes (Figure 2 and Additional file 1: Figure S5). Some of the replicates of the membrane systems with long-chain GPLs were elongated to 500 ns, confirming that 200-300 ns were sufficient time windows to reach the stabilization of the properties of interest (Table 1, Additional file 1: Figure S6).

All the scripts, inputs and outputs, and the documentation required to reproduce the simulations and analyses described in this paper are freely available at the GitHub repository: https://github.com/ELELAB/YEAST_MEMBRANE_MD. The MD trajectories are freely available as OSF repository at https://osf.io/3j2ap/

4.2. Strains and cultivation media

Escherichia coli strain NEB5α (C2987H, New England Biolabs) was used for plasmid propagation and safekeeping. The strain was grown on Lysogeny Broth medium (10 g/l peptone, 5 g/l yeast extract, 5 g/l NaCl with 15 g/l agar). In transformation reactions, the medium was appropriately supplemented with antibiotics (100 µg/ml ampicillin, 25 µg/ml chloramphenicol, 50 µg/ml kanamycin or G418).

S. cerevisiae strain CEN.PK113_5D (45) was grown on complex medium (YPD medium, 20 g/l peptone, 10 g/l yeast extract, 20 g/l glucose, 15 g/l agar) prior to genetic modification. Transformants were selected on synthetic dropout medium (20 g/l glucose, 5 g/l $(NH_4)_2SO_4$, 1.7 g/l yeast nitrogen base, 0.77 g/l nutritional supplement mixture minus uracil (FORMEDIUM, Norfolk, UK), 20 g/l agar) and transformants were subsequently grown on defined medium (46) adjusted to pH 5 using potassium hydroxide and buffered using 50 mM potassium hydrogen phthalate.

4.3. Plasmid construction

Synthetic, codon-optimised versions of FAE1 and GPAT5 were obtained (TWIST Bioscience, CA, USA) and integrated into plasmids using modular cloning for *S. cerevisiae* (26) (Addgene kit #1000000061). Single gene expression plasmids were expressed in *S. cerevisiae* as plasmid. Multigene expression vectors and the empty plasmid control (EPC) were integrated into the genome using site-directed integration into the *ura*3-52 mutation of *S. cerevisiae* strain CEN.PK113_5D whilst creating prototrophic transformants. Plasmid maps as well as codon optimised gene sequences are available in the Supplementary Material.

4.4. *Saccharomyces cerevisiae* transformation

S. cerevisiae transformation was performed using the PEG-mediated LiOAc method based on Giezt and Woods (47). No cell titer was used, as instead an initial OD_{600} of 0.4 was used and cells were harvested at OD_{600} 1.0-1.5. Harvested and washed cells were resuspended in 1 ml of 0.1 M LiOAc. For each transformation, 100 µl was transferred into a microcentrifuge tube and centrifuged at 6000 G for 30 s after which the supernatant was removed. The reactions were placed on ice and the following was added in order to each reaction: 240 µl 50% PEG4000, 35 µl 1 M LiOAc, 75 µl DNA mix containing the transformation plasmid (<5 µg) and 50 µg of single stranded salmon sperm DNA.

4.5. Lipid screening

The relative chain length of the transformants´ total lipids was preliminarily assessed using standard fatty acid methyl esterification and gas chromatography, to analyse acyl chains lengths of C6-24, as previously described (48).

4.6. Lipidomics

4.6.1. Sample preparation

A single colony of *S. cerevisiae* was taken from <3-day-old defined medium plates and used to inoculate a 50 ml tube containing 15 ml defined medium for overnight incubation at 30 °C, and 200 rpm. A 500 ml baffled shake flask containing 50 ml defined medium was inoculated to an OD_{600} of 0.05, and subsequently incubated at 30 °C, and 160 rpm until an OD_{600} of 0.8 (±0.03) was reached. The flask was placed in an ice water bath for about 15 min. After cooling, 24 ml of the culture was transferred to a separate 50 ml conical tube and centrifuged (4000 G, 5 min, 4 °C). The pellet was flash-frozen in liquid nitrogen prior to storage at –80 °C. The analysis was performed in triplicate for each strain.

Pellets were resuspended in 1 ml sterile Milli Q water and transferred to fresh Fastprep tubes (0.5 mm zirconium beads, Precellys®, Bertin Instruments) on ice, and cell lysis was performed using a Precellys® Evolution cell disruptor (Bertin Instruments) with five cycles of 20 s, at 6800 rpm. The Fastprep tubes were incubated on ice for 1 min between each cycle. After cell disruption, the samples were centrifuged at maximum speed for 1 min. Following this, 0.5 ml was transferred to fresh microcentrifuge tubes, flash-frozen and stored at –80 °C. All samples were transported on dry ice to Lipotype GmbH (Tatzberg, Germany) where shotgun lipidomics were performed on total lipids, according to the premium analysis package.

4.6.2. Lipid extraction for mass spectrometry lipidomics

Mass spectrometry-based lipid analysis was performed by Lipotype GmbH as described previously (13,49). Lipids were extracted using a two-step chloroform/methanol procedure (13). Samples were spiked with an internal lipid standard mixture containing: cytidine diphosphate diacylglycerol (CDP-DAG) 17:0/18:1, Cer 18:1;2/17:0, DAG 17:0/17:0, lysophosphatidate 17:0 (LPA), lyso-phosphatidylcholine 12:0 (LPC), lysophosphatidyl-

ethanolamine 17:1 (LPE), lyso-phosphatidylinositol 17:1 (LPI), lysophosphatidylserine 17:1 (LPS), PA 17:0/14:1, PC 17:0/14:1, PE 17:0/14:1, PG 17:0/14:1, PI 17:0/14:1, PS 17:0/14:1, EE 13:0, TAG 17:0/17:0/17:0, stigmastatrienol, IPC 44:0;2, MIPC 44:0;2 and $M(IP)_2C$ 44:0;2. After extraction, the organic phase was transferred to an infusion plate and dried in a speed vacuum concentrator. First-step dry extract was re-suspended in 7.5 mM ammonium acetate in chloroform/methanol/propanol (1:2:4, V:V:V) and second-step dry extract in a 33% ethanol solution of methylamine in chloroform/methanol (0.003:5:1; V:V:V). All liquid handling steps were performed using a Hamilton Robotics STARlet robotic platform with the Anti Droplet Control feature for organic solvent pipetting.

4.6.3. Mass Spectrometer data acquisition

Samples were analysed by direct infusion on a QExactive mass spectrometer (MS) (Thermo Scientific) equipped with a TriVersa NanoMate ion source (Advion Biosciences). Samples were analysed in both positive and negative ion modes with a resolution of $R_{m/z=200}$=280 000 for MS and $R_{m/z=200}$=17 500 for MS/MS experiments, in a single acquisition. MS/MS was triggered by an inclusion list encompassing corresponding MS mass ranges scanned in 1 Da increments (50). Both MS and MS/MS data were combined to monitor EE, DAG and TAG ions as ammonium adducts, PC as an acetate adduct, and CL, PA, PE, PG, PI and PS as deprotonated anions. MS only was used to monitor LPA, LPE, LPI, LPS, IPC, MIPC and $M(IP)_2C$ as deprotonated anions, and Cer and LPC as acetate adducts.

4.6.4. Data analysis and post-processing

Data were analysed with in-house developed lipid identification software based on LipidXplorer (51,52). Data post-processing and normalization were performed using an in-house developed data management system. Only lipid identifications with a signal-to-noise

ratio >5, and a signal intensity 5-fold higher than in corresponding blank samples were considered for further data analysis.

4.7. Acetic acid uptake and kinetic measurements

4.7.1. Cell cultivation

A single colony of *S. cerevisiae* was taken from <3-day-old defined medium plates and used to inoculate a 50 ml tube containing 10 ml defined medium for overnight incubation at 30˚C, 200 rpm). A 1-l baffled shake flask containing 0.1 l defined medium was inoculated to an OD_{600} of 0.05. Flasks were incubated at 30 °C, 160 rpm until the OD_{600} reached 0.8 (±0.03). Thereafter, 90 ml of cells was harvested and centrifuged at 4 °C, 4000 G, for 5 min. The cells were washed twice using ice-cold 50 mM potassium hydrogen phthalate buffer (pH 5.0). The final pellet was resuspended in 800 µl ice-cold potassium hydrogen phthalate buffer (50 mM, pH 5.0) and stored on ice until analysis (<3 h).

4.7.2. Determination of acetic acid diffusion rate and kinetics

The acetic acid diffusion rate was measured as described previously (4), but using total acetic acid concentrations of 0.56, 2.4, 20 and 144 mM. MATLAB was used to create rational regression lines and confidence intervals.

Next, acetic acid diffusion kinetics were determined using a final amount of 7.4-51.8 kBq (0.148-1.036 Bq/µl) [1-^{14}C] acetic acid mixed with 0.2-1.4 mM non-radiolabelled acetic acid, resulting in total acetic acid concentrations of 0.27-1.9 mM, with a specific activity of 39300 DPM/nmol. Each assay was initiated by incubating 10 µl of cells stored on ice with 30 µl of 50 mM potassium hydrogen phthalate buffer at pH 5.0, in a 30° C water bath for 4 min. Acetic acid diffusion was then measured after the addition of 10 µl acetic acid mixture by incubation at 30˚C for 30 s. At this time, the assay was terminated by addition of 10 ml ice-

cold 2 mM acetic acid stop solution. The cells were swiftly filtered and handled as described above. The wash solution used was ice-cold 2 mM acetic acid.

4.7.3. Analysis of intracellular acetic acid concentration

The amount of intracellular acetic acid was determined by measuring the radioactive decay of [^{14}C] acetic acid using a liquid scintillation counter (Wallac Guardian 1414, Perkin Elmer). Background radiation was measured in cultures, scintillation liquid and the filters used in a representative way. None of the background controls showed significant amounts of radioactivity, and the average background was subtracted from the samples. The radioactive decay measured was within the linear concentration range and no quenching effects of the sample matrix were observed.

4.8. Cultivation of *Saccharomyces cerevisiae* in a growth profiler

S. cerevisiae inoculum was prepared in a 96-well plate (Tissue Culture Testplate®, SPL Life Sciences) containing 150 µl defined medium at pH 5. The culture was grown overnight in a thermomixer (Eppendorf ThermoTop®) at 30 °C, 200 rpm. Cells were resuspended by pipetting prior to measurement of the cell density using a plate reader (Spectrostar Nano®, BMG Labtech). The cells were then transferred to a fresh 96-well plate (CR1496e®, System Duetz) with a final volume of 200 µl and starting OD_{600}-equivalent of 0.02. Strain analysis was performed in triplicate. The plate was sealed with a machine-specific aerobic sandwich cover (CR1296a EnzyScreen B.V.). The plate was incubated in a growth profiler (GP960 REV2®, EnzyScreen) for 72 h at 30 °C, 230 rpm, and green light scattering measurements were taken hourly. Defined medium was used as a blank, and the value of the green light scattering signal (green value, GV) obtained from this was subtracted from the values measured during cell growth.

Green values were converted into OD_{600} values using a standard curve obtained previously using *S. cerevisiae* strain CENPK_113.7D (45) grown in defined medium. The following two equations were used to convert GV into OD_{600} values:

For GV ≤ 10:

$$OD600 = 0.0322\ x\ 2.72^{(0.4328\ x\ GV)} \quad (3)$$

For GV ≥ 10:

$$OD600 = -0.0004\ x\ GV^3 + 0.0398\ x\ GV^2 - 0.6506\ x\ GV + 5.4063 \quad (4)$$

5. List of abbreviations

AOPC	1-arachidoyl-2-oleoyl-sn-glycero-3-phosphocholine
AOPI	1-arachidoyl-2-oleoyl-sn-glycero-3-phospho-(1'-myo-inositol)
APL	area per lipid
BOPC	1-behenoyl-2-oleoyl-sn-glycero-3-phosphocholine
BOPI	1-behenoyl-2-oleoyl-sn-glycero-3-phospho-(1'-myo-inositol)
CDP-DAG	cytidine diphosphate diacylglycerol
Cer	ceramide
CL	cardiolipin
DAG	diacylglycerol
DOPC	1,2-dioleoyl-sn-glycerol-3-phosphocholine
EE	ergosterol ester
EPC	empty plasmid control
ERG	ergosterol
FA	fatty acid
GPAT	glycerol-3-phosphate acyl transferase
GPL	glycerophospholipid
GV	green value
IPC	inositol phosphorylceramide

L-GPL	lyso-glycerophospholipid
LOPC	1-lignoceroyl-2-oleoyl-sn-glycero-3-phosphocholine
LOPI	1-lignoceroyl-2-oleoyl-sn-glycero-3-phospho-(1'-myo-inositol)
LPA	lysophosphatidate
LPC	lyso-phosphatidylcholine
LPE	lysophosphatidyl-ethanolamine
LPI	lyso-phosphatidylinositol
LPS	lysophosphatidylserine
$M(IP)_2C$	mannosyl-di-(inositol phosphoryl) ceramide
MD	Molecular dynamics
MIPC	mannosyl-inositol phosphorylceramide
MS	mass spectrometer
MT	membrane thickness
PA	phosphatidic acid
PC	phosphatidylcholine
PE	phosphatidyl-ethanolamine
PG	phosphatidylglycerol
PI	phosphatidylinositol
PM	plasma membrane
POPI	1-palmitoyl-2-oleoyl-sn-glycerol-3-phospho-(1'-myo-inositol)
PS	phosphatidylserine
S_{CD}	Deuterium order parameter
Slipds ff	Stockholm lipids force field
TAG	triacylglycerol

6. Declarations

Ethics approval and consent to participate

Not applicable

Consent for publication

Not applicable

Availability of data and materials

All the scripts, inputs and outputs, and the documentation required to reproduce the molecular dynamics simulations and analyses used in this article are available in the GitHub repository: https://github.com/ELELAB/YEAST_MEMBRANE_MD.

The MD trajectories analysed during this study are available as OSF repository at https://osf.io/3j2ap/

The raw lipid data obtained through Lipotype GmbH is included in this published article as comma delimited file (Additional file 2)

Supplementary data required to reproduce the work presented or supporting the conclusions of the current study are included in this published article (Additional file 1).

Competing interests

The authors declare that they have no competing interests

Funding

This work was supported by the Swedish Energy Agency [grant number 43524-1] and the Swedish Research Council for Sustainable Development FORMAS [grant number 2018-1023]. EP group is part of the Center of Excellence in Autophagy, Recycling and Disease (CARD), funded by the Danish National Research Foundation (DNRF125) and also supported by The Danish Council for Independent Research, Natural Science Research Project 1 (102517). The calculations described in this paper were performed using resources provided by the

Swedish National Infrastructure for Computing (SNIC) at PDC Center for High Performance Computing under the project SNIC 2019/8-69.

Authors´ contributions

JMM aided in conceptualisation and project management. JMM performed experimental design and executed wet-lab experiments. SS performed the MD simulations and analysed them. ML aided in the supervision and data analysis of the computational part of the project. SG wrote and validated the simulation scripts. CT performed growth profiler experiments. LAE aided in the supervision of the computational part of the project. EP was involved in the discussion and interpretation of the simulation data and aided in the supervision of the computational part. LO aided in funding acquisition, supervision and discussion of the results. MB aided in funding acquisition, conceptualisation, project administration and supervision of this research. JMM wrote and revised the bulk of the article and SS, ML, CT, EL, LO and MB all contributed to writing and revising of the article.

Acknowledgements

We would like to thank Fábio Luis Da Silva Faria Oliveira, who was an invaluable help to the wet-lab part of this study. Furthermore, we would like to thank Stefan Allard for his help regarding radioactivity and the acetic acid uptake measurements. We would also like to thank David Nickel and Vera Novy for their help and input.

References

1. Jönsson LJ, Martín C. Pretreatment of lignocellulose: Formation of inhibitory by-products and strategies for minimizing their effects. Bioresource Technology. 2016. DOI: 10.1016/j.biortech.2015.10.009
2. Giannattasio S, Guaragnella N, Corte-Real M, Passarella S, Marra E. Acid stress adaptation protects Saccharomyces cerevisiae from acetic acid-induced programmed cell death. In: Gene. 2005. DOI: 10.1016/j.gene.2005.03.030
3. Ludovico P, Rodrigues F, Almeida A, Silva MT, Barrientos A, Côrte-Real M. Cytochrome

c release and mitochondria involvement in programmed cell death induced by acetic acid in Saccharomyces cerevisiae. Mol Biol Cell. 2002; DOI: 10.1091/mbc.E01-12-0161

4. Lindahl L, Genheden S, Faria-Oliveira F, Allard S, Eriksson LA, Olsson L, et al. Alcohols enhance the rate of acetic acid diffusion in S. Cerevisiae: Biophysical mechanisms and implications for acetic acid tolerance. Microb Cell. 2018; DOI: 10.15698/mic2018.01.609

5. Orij R, Brul S, Smits GJ. Intracellular pH is a tightly controlled signal in yeast. Biochimica et Biophysica Acta - General Subjects. 2011. DOI: 10.1016/j.bbagen.2011.03.011

6. J. M, Ludovico P, Rodrigues F, Leo C, Crte-Real M. Stress and Cell Death in Yeast Induced by Acetic Acid. In: Cell Metabolism - Cell Homeostasis and Stress Response. 2012. DOI: 10.5772/27726

7. Russell JB. Another explanation for the toxicity of fermentation acids at low pH: anion accumulation versus uncoupling. Journal of Applied Bacteriology. 1992. DOI: 10.1111/j.1365-2672.1992.tb04990.x

8. Rodrigues F, Sousa MJ, Ludovico P, Santos H, Côrte-Real M, Leão C. The Fate of Acetic Acid during Glucose Co-Metabolism by the Spoilage Yeast Zygosaccharomyces bailii. PLoS One. 2012; DOI: 10.1371/journal.pone.0052402

9. Ullah A, Chandrasekaran G, Brul S, Smits GJ. Yeast adaptation to weak acids prevents futile energy expenditure. Front Microbiol. 2013; DOI: 10.3389/fmicb.2013.00142

10. Van der Rest ME, Kamminga AH, Nakano A, Anraku Y, Poolman B, Konings WN. The plasma membrane of Saccharomyces cerevisiae: Structure, function, and biogenesis. Microbiological Reviews. 1995.

11. Alwarawrah M, Hussain F, Huang J. Alteration of lipid membrane structure and dynamics by diacylglycerols with unsaturated chains. Biochim Biophys Acta - Biomembr. 2016; DOI: 10.1016/j.bbamem.2015.11.014

12. Henry SA, Kohlwein SD, Carman GM. Metabolism and regulation of glycerolipids in the yeast Saccharomyces cerevisiae. Genetics. 2012; DOI: 10.1534/genetics.111.130286

13. Ejsing CS, Sampaio JL, Surendranath V, Duchoslav E, Ekroos K, Klemm RW, et al. Global analysis of the yeast lipidome by quantitative shotgun mass spectrometry. Proc Natl Acad Sci. 2009; DOI: 10.1073/pnas.0811700106

14. Kobayashi SD, Nagiec MM. Ceramide/long-chain base phosphate rheostat in Saccharomyces cerevisiae: Regulation of ceramide synthesis by Elo3p and Cka2p. Eukaryot Cell. 2003; DOI: 10.1128/EC.2.2.284-294.2003

15. Renne MF, de Kroon AIPM. The role of phospholipid molecular species in determining the physical properties of yeast membranes. FEBS Letters. 2018. DOI: 10.1002/1873-3468.12944

16. Qi Y, Liu H, Chen X, Liu L. Engineering microbial membranes to increase stress tolerance of industrial strains. Metabolic Engineering. 2019. DOI: 10.1016/j.ymben.2018.12.010

17. Kajiwara S, Aritomi T, Suga K, Ohtaguchi K, Kobayashi O. Overexpression of the OLE1 gene enhances ethanol fermentation by Saccharomyces cerevisiae. Appl Microbiol Biotechnol. 2000; DOI: 10.1007/s002530051658

18. Lindahl L, Santos AXS, Olsson H, Olsson L, Bettiga M. Membrane engineering of S. cerevisiae targeting sphingolipid metabolism. Sci Rep. 2017; DOI: 10.1038/srep41868

19. Endo S, Escher BI, Goss KU. Capacities of membrane lipids to accumulate neutral organic chemicals. Environmental Science and Technology. 2011. DOI: 10.1021/es200855w

20. Trenkamp S, Martin W, Tietjen K. Specific and differential inhibition of very-long-chain fatty acid elongases from Arabidopsis thaliana by different herbicides. Proc Natl Acad Sci U S A. 2004; DOI: 10.1073/pnas.0404600101

21. Chen X, Snyder CL, Truksa M, Shah S, Weselake RJ. Sn-glycerol-3-phosphate acyltransferases in plants. Plant Signaling and Behavior. 2011. DOI: 10.4161/psb.6.11.17777

22. Lindahl L, Genheden S, Eriksson LA, Olsson L, Bettiga M. Sphingolipids contribute to acetic acid resistance in Zygosaccharomyces bailii. Biotechnol Bioeng. 2016; DOI: 10.1002/bit.25845

23. De Kroon AIPM, Rijken PJ, De Smet CH. Checks and balances in membrane phospholipid class and acyl chain homeostasis, the yeast perspective. Progress in Lipid Research. 2013. DOI: 10.1016/j.plipres.2013.04.006

24. Yeagle PL. Lipid Dynamics in Membranes. In: The Membranes of Cells. 2016. DOI: 10.1016/b978-0-12-800047-2.00008-5

25. Lindberg L, Santos AXS, Riezman H, Olsson L, Bettiga M. Lipidomic Profiling of Saccharomyces cerevisiae and Zygosaccharomyces bailii Reveals Critical Changes in Lipid Composition in Response to Acetic Acid Stress. PLoS One. 2013; DOI: 10.1371/journal.pone.0073936

26. Lee ME, DeLoache WC, Cervantes B, Dueber JE. A Highly Characterized Yeast Toolkit for Modular, Multipart Assembly. ACS Synth Biol. 2015; DOI: 10.1021/sb500366v

27. Simons K, Sampaio JL. Membrane organization and lipid rafts. Cold Spring Harbor Perspectives in Biology. 2011. DOI: 10.1101/cshperspect.a004697

28. Campomanes P, Zoni V, Vanni S. Local accumulation of diacylglycerol alters membrane properties nonlinearly due to its transbilayer activity. Commun Chem. 2019; DOI: 10.1038/s42004-019-0175-7

29. Ganesan S, Sosa Ponce ML, Tavassoli M, Shabits BN, Mahadeo M, Prenner EJ, et al. Metabolic control of cytosolic-facing pools of diacylglycerol in budding yeast. Traffic. 2019; DOI: 10.1111/tra.12632

30. Megha, London E. Ceramide selectively displaces cholesterol from ordered lipid domains (rafts): Implications for lipid raft structure and function. J Biol Chem. 2004; DOI: 10.1074/jbc.M309992200

31. Abraham MJ, Murtola T, Schulz R, Páll S, Smith JC, Hess B, et al. Gromacs: High performance molecular simulations through multi-level parallelism from laptops to

supercomputers. SoftwareX. 2015; DOI: 10.1016/j.softx.2015.06.001

32. Jämbeck JPM, Lyubartsev AP. An extension and further validation of an all-atomistic force field for biological membranes. J Chem Theory Comput. 2012; DOI: 10.1021/ct300342n

33. Jämbeck JPM, Lyubartsev AP. Derivation and systematic validation of a refined all-atom force field for phosphatidylcholine lipids. J Phys Chem B. 2012; DOI: 10.1021/jp212503e

34. Jämbeck JPM, Lyubartsev AP. Another piece of the membrane puzzle: Extending slipids further. J Chem Theory Comput. 2013; DOI: 10.1021/ct300777p

35. Jorgensen WL, Chandrasekhar J, Madura JD, Impey RW, Klein ML. Comparison of simple potential functions for simulating liquid water. J Chem Phys. 1983; DOI: 10.1063/1.445869

36. Wu EL, Cheng X, Jo S, Rui H, Song KC, Dávila-Contreras EM, et al. CHARMM-GUI membrane builder toward realistic biological membrane simulations. Journal of Computational Chemistry. 2014. DOI: 10.1002/jcc.23702

37. Hess B, Bekker H, Berendsen HJC, Fraaije JGEM. LINCS: A Linear Constraint Solver for molecular simulations. J Comput Chem. 1997; DOI: 10.1002/(SICI)1096-987X(199709)18:12<1463::AID-JCC4>3.0.CO;2-H

38. Parrinello M, Rahman A. Crystal structure and pair potentials: A molecular-dynamics study. Phys Rev Lett. 1980; DOI: 10.1103/PhysRevLett.45.1196

39. Hoover WG, Holian BL. Kinetic moments method for the canonical ensemble distribution. Phys Lett Sect A Gen At Solid State Phys. 1996; DOI: 10.1016/0375-9601(95)00973-6

40. Darden T, York D, Pedersen L. Particle mesh Ewald: An N·log(N) method for Ewald sums in large systems. J Chem Phys. 1993; DOI: 10.1063/1.464397

41. Balusek C, Hwang H, Lau CH, Lundquist K, Hazel A, Pavlova A, et al. Accelerating Membrane Simulations with Hydrogen Mass Repartitioning. J Chem Theory Comput. 2019; DOI: 10.1021/acs.jctc.9b00160

42. Perez JJ, Tomas MS, Rubio-Martinez J. Assessment of the Sampling Performance of Multiple-Copy Dynamics versus a Unique Trajectory. J Chem Inf Model. 2016; DOI: 10.1021/acs.jcim.6b00347

43. Caves LSD, Evanseck JD, Karplus M. Locally accessible conformations of proteins: Multiple molecular dynamics simulations of crambin. Protein Sci. 1998; DOI: 10.1002/pro.5560070314

44. Poger D, Caron B, Mark AE. Validating lipid force fields against experimental data: Progress, challenges and perspectives. Biochim Biophys Acta - Biomembr. 2016; DOI: 10.1016/j.bbamem.2016.01.029

45. Entian KD, Kötter P. 25 Yeast Genetic Strain and Plasmid Collections. Methods in Microbiology. 2007. DOI: 10.1016/S0580-9517(06)36025-4

46. Verduyn C, Postma E, Scheffers WA, Van Dijken JP. Effect of benzoic acid on metabolic fluxes in yeas... [Yeast. 1992] - PubMed result. Yeast. 1992; DOI:

10.1002/yea.320080703

47. Gietz RD, Woods RA. Transformation of yeast by lithium acetate/single-stranded carrier DNA/polyethylene glycol method. Methods Enzymol. 2002; DOI: 10.1016/S0076-6879(02)50957-5

48. Khoomrung S, Chumnanpuen P, Jansa-Ard S, Nookaew I, Nielsen J. Fast and accurate preparation fatty acid methyl esters by microwave-assisted derivatization in the yeast Saccharomyces cerevisiae. Appl Microbiol Biotechnol. 2012; DOI: 10.1007/s00253-012-4125-x

49. Klose C, Surma MA, Gerl MJ, Meyenhofer F, Shevchenko A, Simons K. Flexibility of a eukaryotic lipidome - insights from yeast lipidomics. PLoS One. 2012; DOI: 10.1371/journal.pone.0035063

50. Surma MA, Herzog R, Vasilj A, Klose C, Christinat N, Morin-Rivron D, et al. An automated shotgun lipidomics platform for high throughput, comprehensive, and quantitative analysis of blood plasma intact lipids. Eur J Lipid Sci Technol. 2015; DOI: 10.1002/ejlt.201500145

51. Herzog R, Schwudke D, Schuhmann K, Sampaio JL, Bornstein SR, Schroeder M, et al. A novel informatics concept for high-throughput shotgun lipidomics based on the molecular fragmentation query language. Genome Biol. 2011; DOI: 10.1186/gb-2011-12-1-r8

52. Herzog R, Schuhmann K, Schwudke D, Sampaio JL, Bornstein SR, Schroeder M, et al. Lipidxplorer: A software for consensual cross-platform lipidomics. PLoS One. 2012; DOI: 10.1371/journal.pone.0029851

Figure captions

Figure 1. Membrane composition, acetic acid homeostasis and lipid metabolism.

Membrane composition and structure are illustrated in panel A. The undissociated form of acetic acid can diffuse passively across the lipid bilayer, while the dissociated form is actively removed from the cell by the transporters Pma1 and Tpo3. Chemical equilibrium exists between the dissociated and undissociated forms of acetic acid both inside and outside the cell, depending on the pH (pKa ~ 4.8). Intracellular concentration is dependent on the equilibrium of undissociated form inside and outside the cell. The plasma membrane is composed of cylindrical (sphingolipids, PC, PS, PI) and conically shaped lipids (with a small head: DAG, PA, PE; or a large heard: lyso-glycerophospholipids). A simplified illustration of *S. cerevisiae* lipid metabolism is shown in panel B. The *Arabidopsis thaliana* genes used in

781 strain engineering (*FAE1*, *GPAT5*) are shown in grey. AcCOO-, acetate; AcCOOH, acetic acid,
782 CDP-DAG, cytidine diacylglycerol; Cer, Ceramides; CL, cardiolipin; DAG, diacylglycerol; EE,
783 ergosterol ester; ELO, fatty acid elongation; *FAE1*, (*Arabidopsis thaliana*) fatty acid elongase
784 1; FAS, (*de novo*) fatty acid synthesis; *GPAT5*, (*Arabidopsis thaliana*) glycerol-3-phosphate
785 acyltransferase 5; IPC, inositol phosphorylceramide; $M(IP)_2C$, mannosyl-di-(inositol
786 phosphoryl) ceramide; MIPC, mannosyl-inositol phosphorylceramide; PA, phosphatidic acid;
787 PC, phosphatidylcholine; PE, phosphatidylethanolamine; PG, phosphatidylglycerol; PI,
788 phosphatidylinositol; PS, phosphatidylserine; TAG, triacylglycerol.

789 **Figure 2**. **Long-chain glycerophospholipids increase the packing and rigidity of yeast**
790 **membrane models in a concentration-dependent manner.** Mean values and associated
791 standard deviations of the structural properties of the membranes investigated in this
792 study: A) the area per lipid (APL), B) the membrane thickness (MT) and C and D) the
793 deuterium order parameter (S_{CD}) of the *sn1* acyl chains of DOPC and POPI. Simulations were
794 performed for a membrane system with no long-chain GPLs (indicated as Null) and for
795 membrane systems with increasing concentrations of long-chain GPLs from 8% to 96%. The
796 mean values were calculated based on three replicates per system.

797 **Figure 3. Glycerophospholipid acyl chain length and relative abundance of plasma**
798 **membrane headgroups**. Panel A shows the combined chain length of the two acyl chains of
799 glycerophospholipids obtained from total lipid analysis. The cumulative relative amounts of
800 short- (C24-31), long- (C32-36) and very-long- (C37-48) chain glycerophospholipids are
801 shown in the insert. Panel B shows the relative abundances of membrane lipid headgroups,
802 and the insert shows the cumulated amounts of different lipid classes. Asterisks indicate
803 significant differences at the 95% confidence level. CDP-DAG, cytidine diacylglycerol; Cer,

804 Ceramides; DAG, diacylglycerol; GPL, glycerophospholipid; IPC, inositol phosphorylceramide;
805 L-GPL, lyso-glycerophospholipid; $M(IP)_2C$, mannosyl-di-(inositol phosphoryl) ceramide;
806 MIPC, mannosyl-inositol phosphorylceramide; PA, phosphatidic acid; PC,
807 phosphatidylcholine; PE, phosphatidylethanolamine; PI, phosphatidylinositol; PS,
808 phosphatidylserine; SL, sphingolipid; TAG, triacylglycerol.

809 **Figure 4. Acetic acid uptake with an initial extracellular acetic acid concentration of**
810 **144 mM, pH 5.0.** Rational regression lines were calculated using MATLAB and the 90%
811 confidence intervals are shown by the dotted lines. The average sample response is given at
812 each time point measured (10, 45, 80, 300 and 600 s). The highest intracellular
813 concentration of acetic acid was observed in the EPC control strain (black), while the
814 FAE1_GPAT5 strain showed lower maximum intracellular acetic acid concentrations (grey).

815 **Figure 5. Acetic acid uptake kinetics.** When acetic acid transport occurs by passive diffusion
816 across the plasma membrane, there will be a linear correlation between the extracellular
817 acetic acid concentration (mM, x-axis) and the acetic acid permeation rate (nmol/(mg dry
818 weight x s), y-axis), if the pH is constant. The slope of the regression line is indicative of the
819 net uptake rate, and for FAE1_GPAT5, this was 0.153, while it was 0.118 for EPC. The data
820 confirms that the uptake predominantly occurs by passive diffusion, and it indicates that the
821 FAE1_GPAT5 strain has a higher net rate of uptake of acetic acid.

822 **Table 1. Lipid compositions of the yeast membrane systems.** Eight lipid membrane systems
823 with increasing concentrations (8, 16, 24, 32, 40, 48, 64 and 96%) of different long-chain
824 GPLs (denoted M1 to M8) were constructed, starting from two reference yeast membrane
825 models (denoted NULL-64 and NULL-256, see Materials and Methods section). Long-chain
826 GPLs 1-arachidoyl-2-oleoyl-sn-glycero-3-phosphocholine (AOPC) and 1-arachidoyl-2-oleoyl-

827 sn-glycero-3-phospho-*(1'-myo-inositol)* (AOPI) with the *sn1* acyl chain length of 20 carbons,
828 1-behenoyl-2-oleoyl-sn-glycero-3-phosphocholine (BOPC) and 1-behenoyl-2-oleoyl-sn-
829 glycero-3-phospho-*(1'-myo-inositol)* (BOPI) with the *sn1* acyl chain length of 22 carbons, 1-
830 lignoceroyl-2-oleoyl-sn-glycero-3-phosphocholine (LOPC) and 1-lignoceroyl-2-oleoyl-sn-
831 glycero-3-phospho-*(1'-myo-inositol)* (LOPI) with the *sn1* acyl chain length of 24 carbons,
832 were introduced at a ratio of 4:2:1, by replacing the representatives of PC and PI lipids
833 (DOPC and POPI, respectively). The same concentrations of sterols and sphingolipids (ERG
834 and IPC, respectively) were maintained in each system as in the reference. The content of
835 long-chain GPLs is expressed as a percentage of the total content of GPLs (% GPL, including
836 DOPC, POPI and long-chain GPLs) and the overall number of lipid molecules (% Tot). The
837 total number of lipid molecules (Lipids) and atoms in each membrane model (N_{tot}) are also
838 reported. Two to five replicates (No. of replicates) of molecular dynamics (MD) simulations
839 were performed for each system, each of 200-500 ns length.

840 **Figure 1. Membrane composition, acetic acid homeostasis and lipid metabolism.**

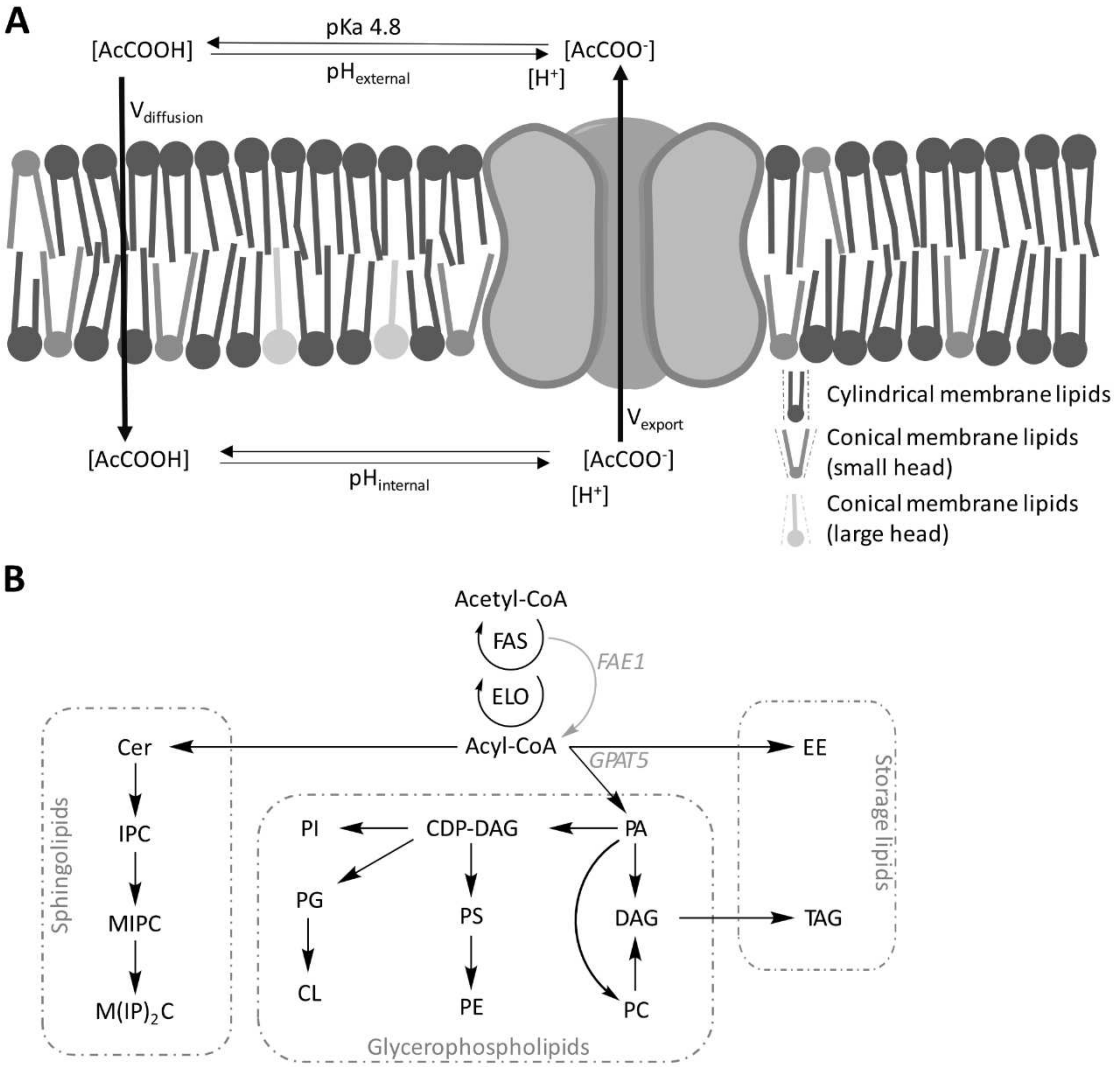

841

842

Figure 2. **Long-chain glycerophospholipids increase the packing and rigidity of yeast membrane models in a concentration-dependent manner.**

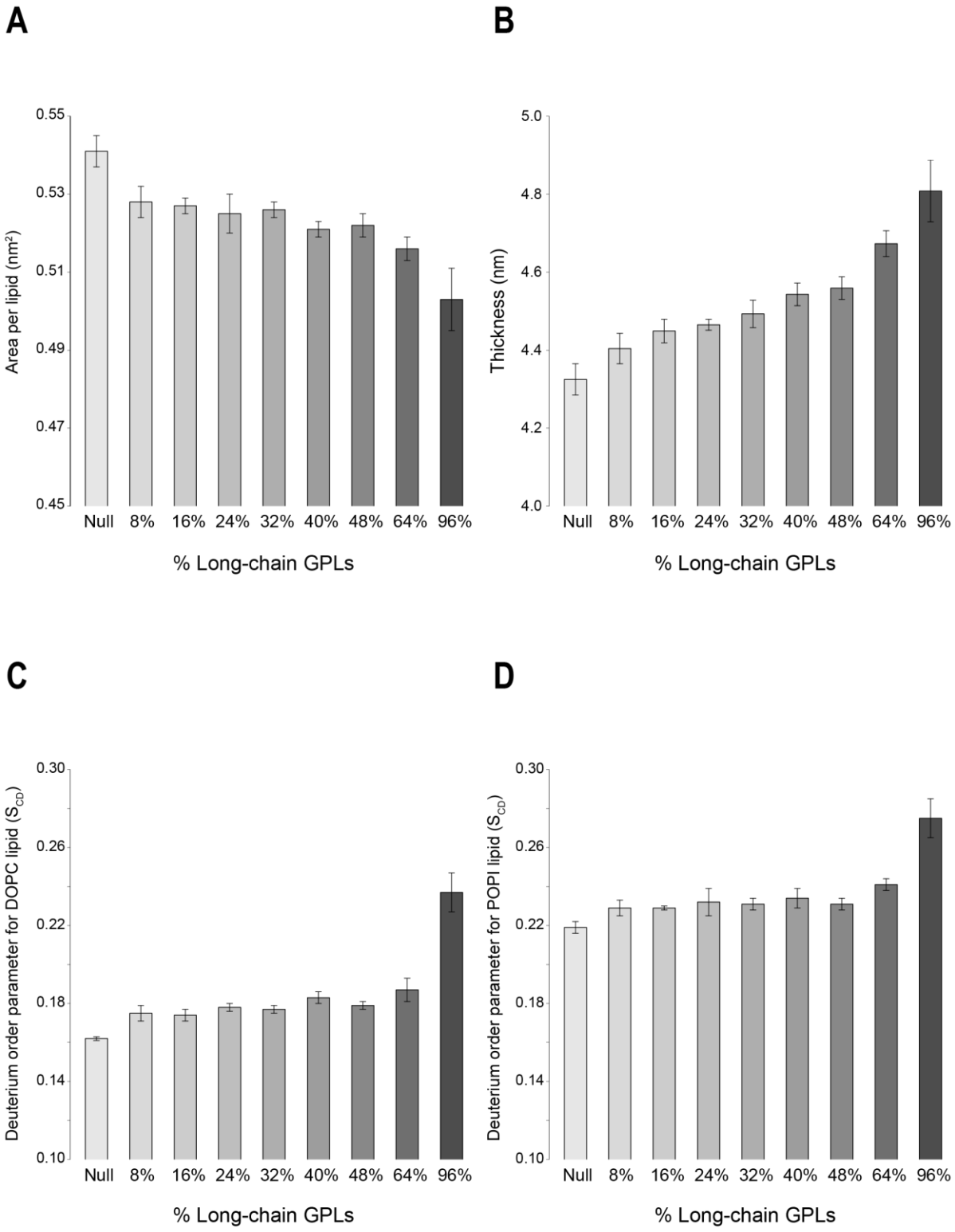

Figure 3. Glycerophospholipid acyl chain length and relative abundance of plasma membrane headgroups.

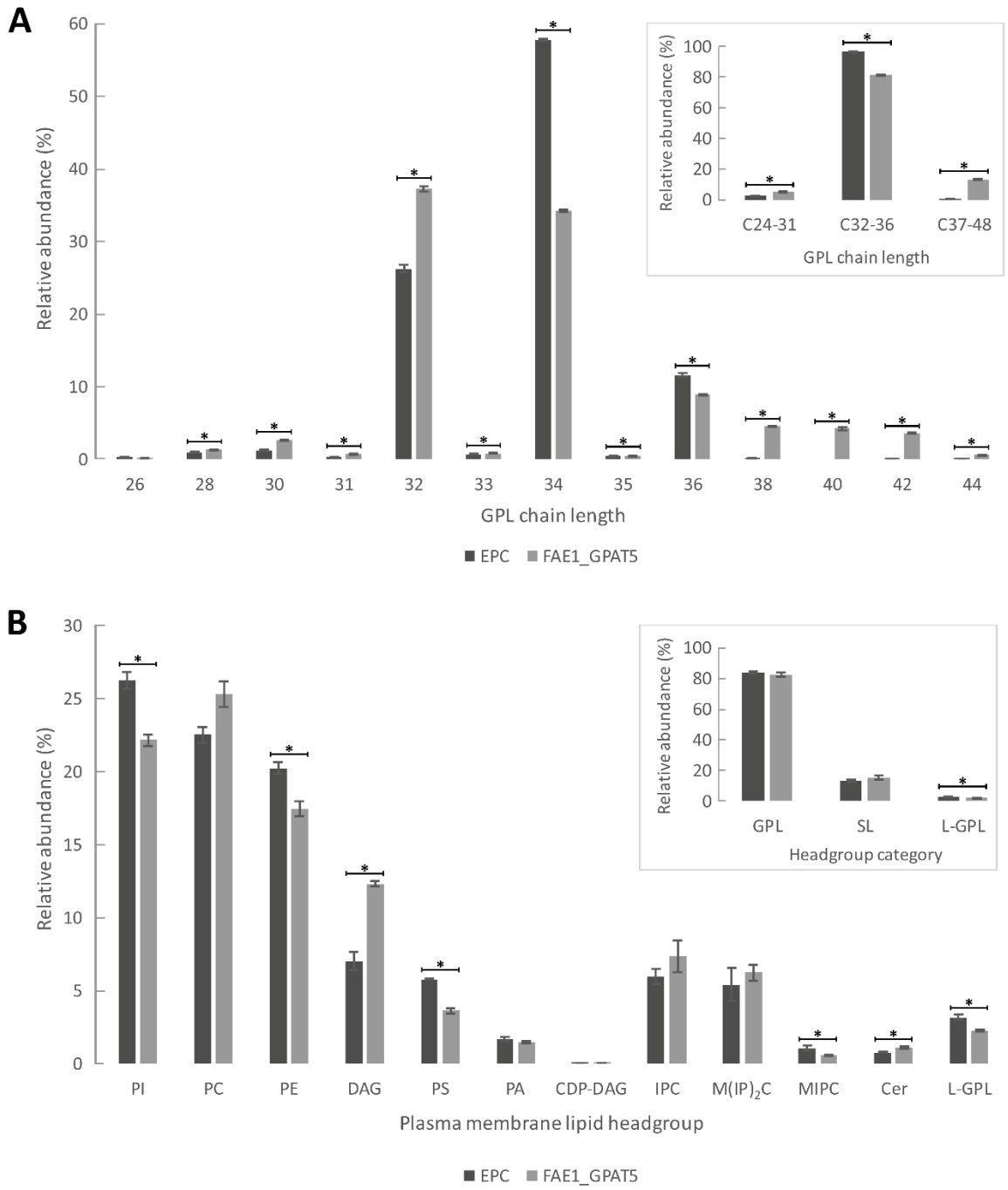

Figure 4. Acetic acid uptake with an initial extracellular acetic acid concentration of 144 mM, pH 5.0.

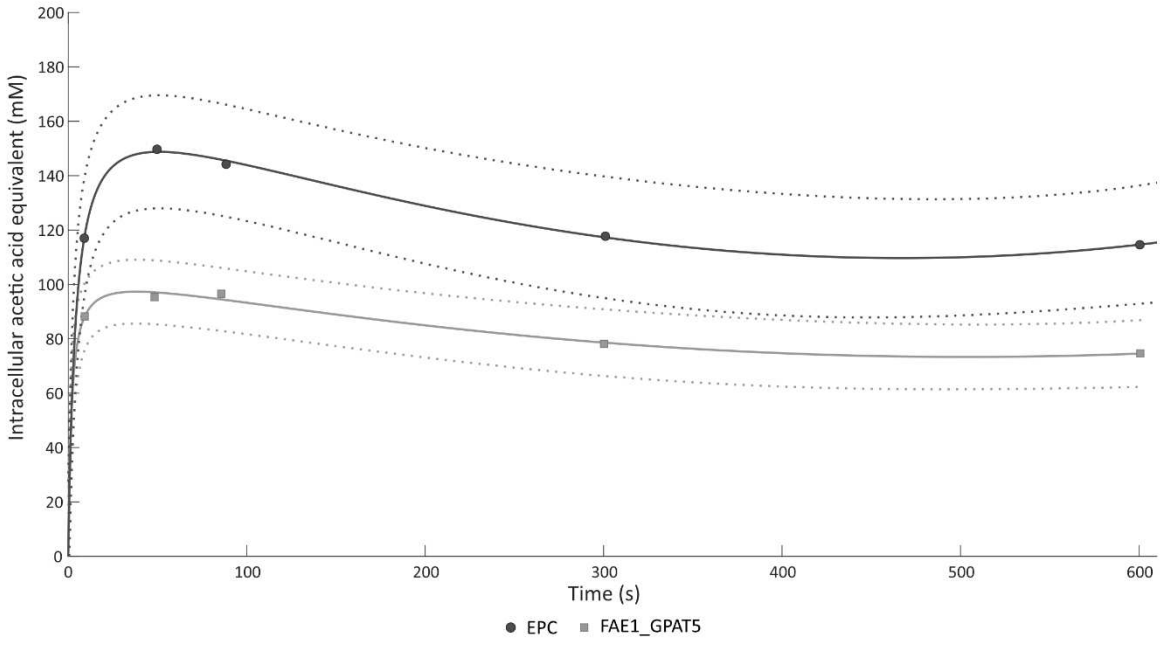

855 **Figure 5. Acetic acid uptake kinetics.**

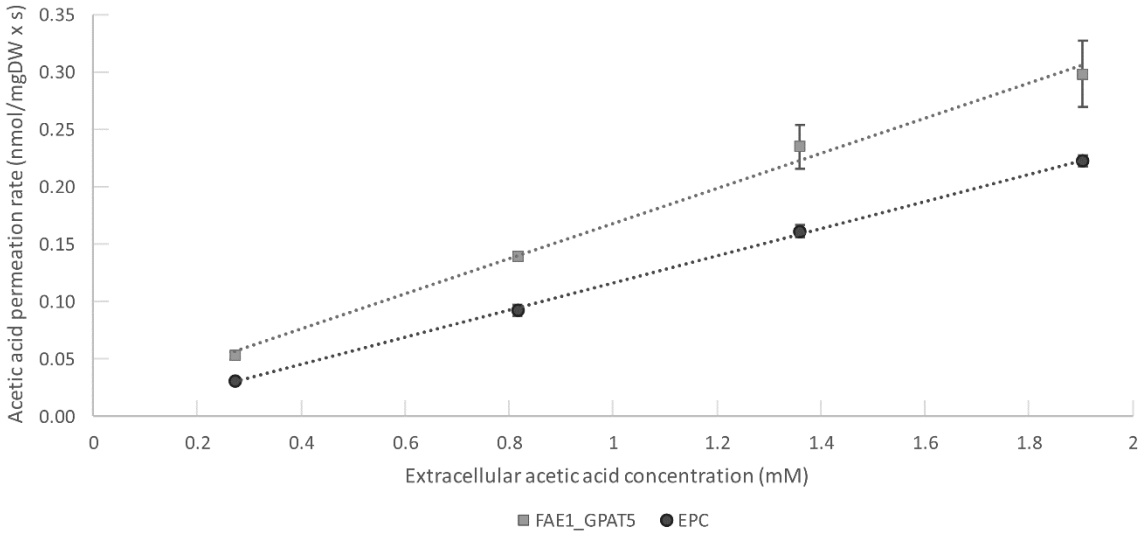

856

857

858 **Table 1. Lipid compositions of the yeast membrane systems.**

Systems	ERG	IPC	DOPC	POPI	AOPC /AOPI	BOPC /BOPI	LOPC /LOPI	Lipids	Ntot	Long chain GPL %	% tot	N° Replicates	Lenght
NULL 64	10	10	22	22	0	0	0	64	16192	0%	0%	1	200ns
NULL 256	40	40	88	88	0	0	0	256	64768	0%	0%	4	200ns
M1	40	40	81	81	4	2	1	256	64956	8%	5%	4	500ns
M2	40	40	74	74	8	4	2	256	65144	16%	11%	4	500ns
M3	40	40	67	67	12	6	3	256	65332	24%	16%	4	500ns
M4	40	40	60	60	16	8	4	256	65520	32%	22%	4	500ns
M5	40	40	53	53	20	10	5	256	65708	40%	27%	5	500ns
M6	40	40	46	46	24	12	6	256	65896	48%	33%	3	300ns (2) - 500ns (1)
M7	40	40	32	32	32	16	8	256	66272	64%	44%	3	300ns (1) - 500ns (1)
M8	40	40	4	4	48	24	12	256	67024	96%	66%	3	300ns (1) - 500ns (2)

859

Figures

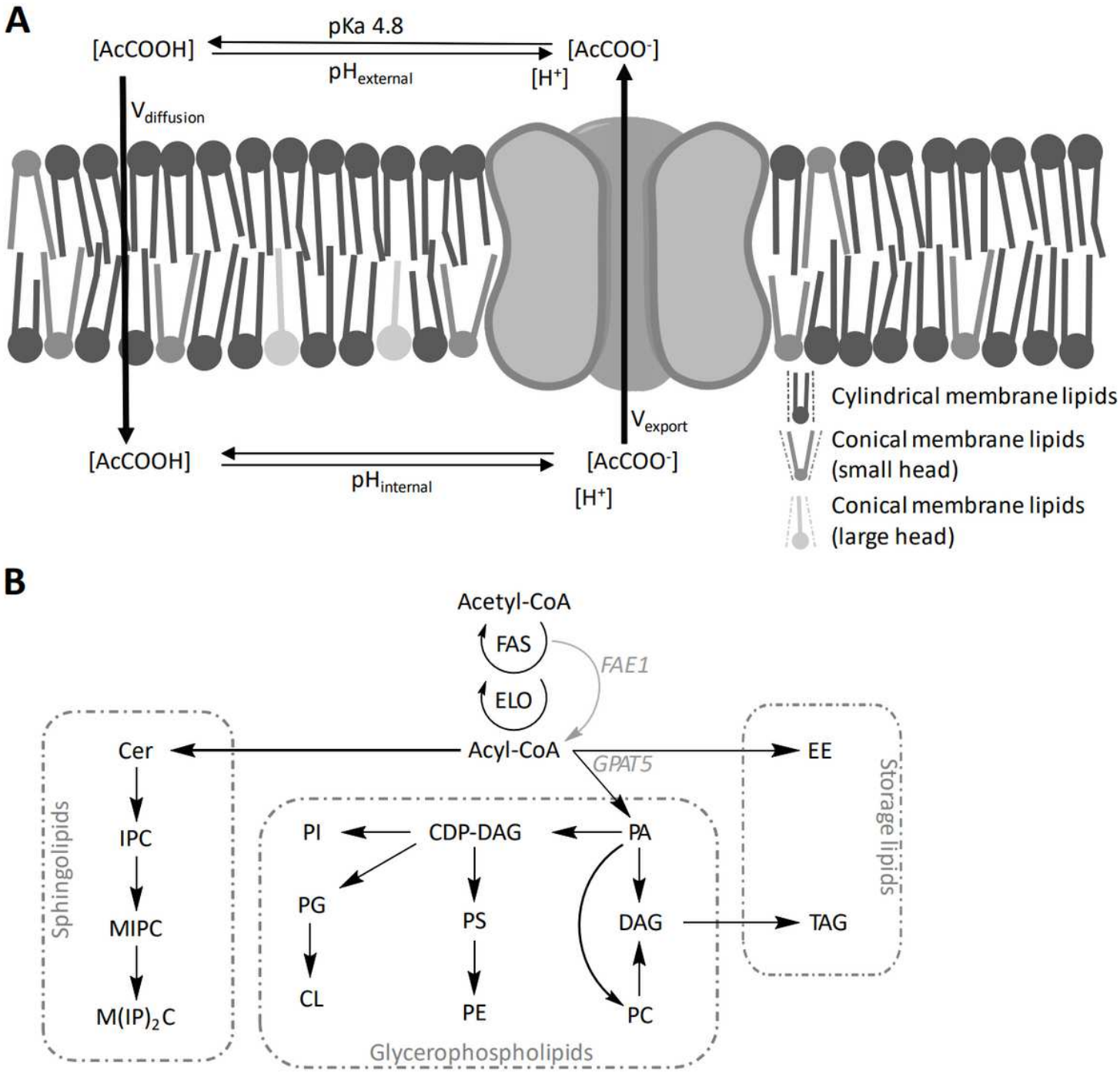

Figure 1

Membrane composition, acetic acid homeostasis and lipid metabolism.

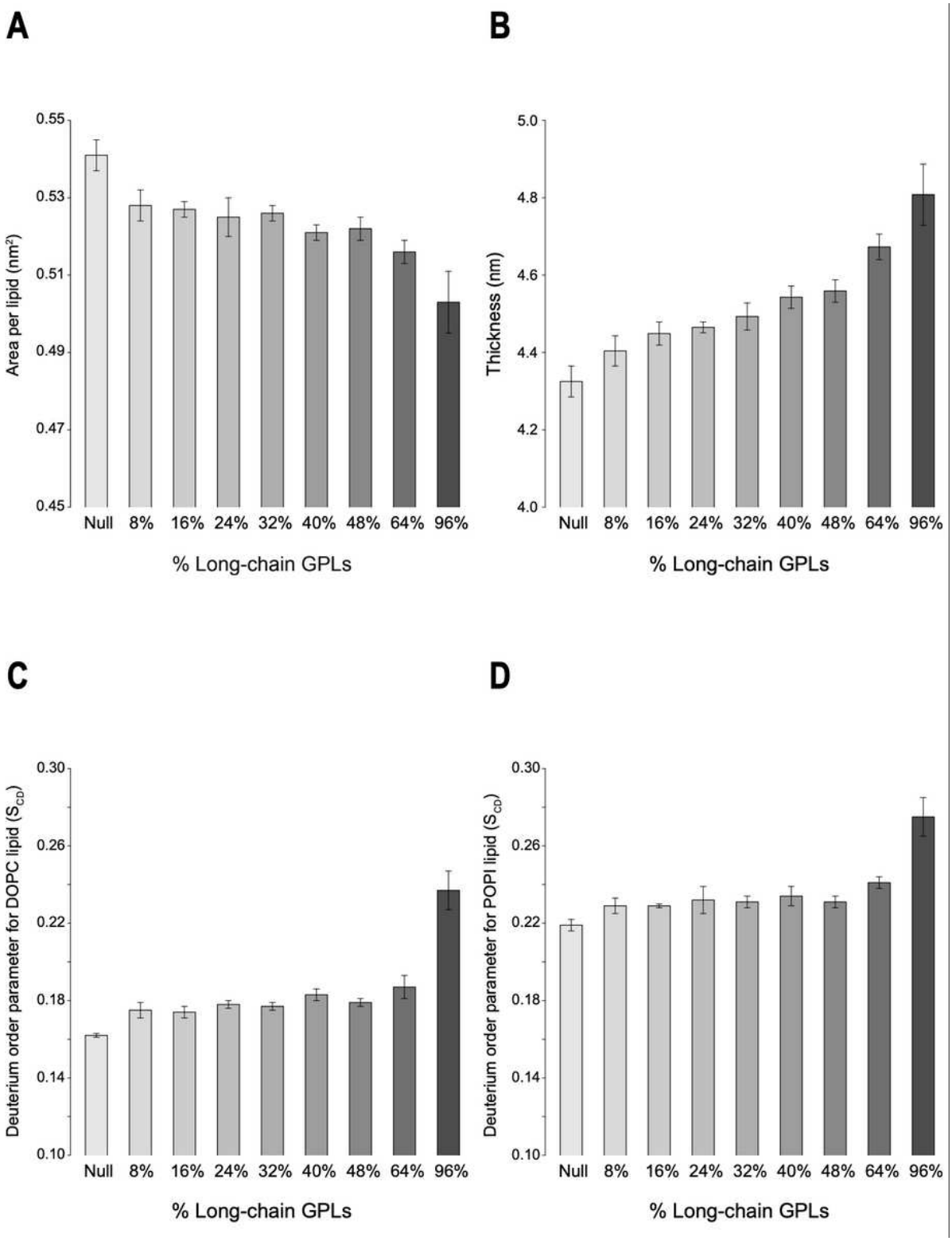

Figure 2

Long-chain glycerophospholipids increase the packing and rigidity of yeast membrane models in a concentration-dependent manner

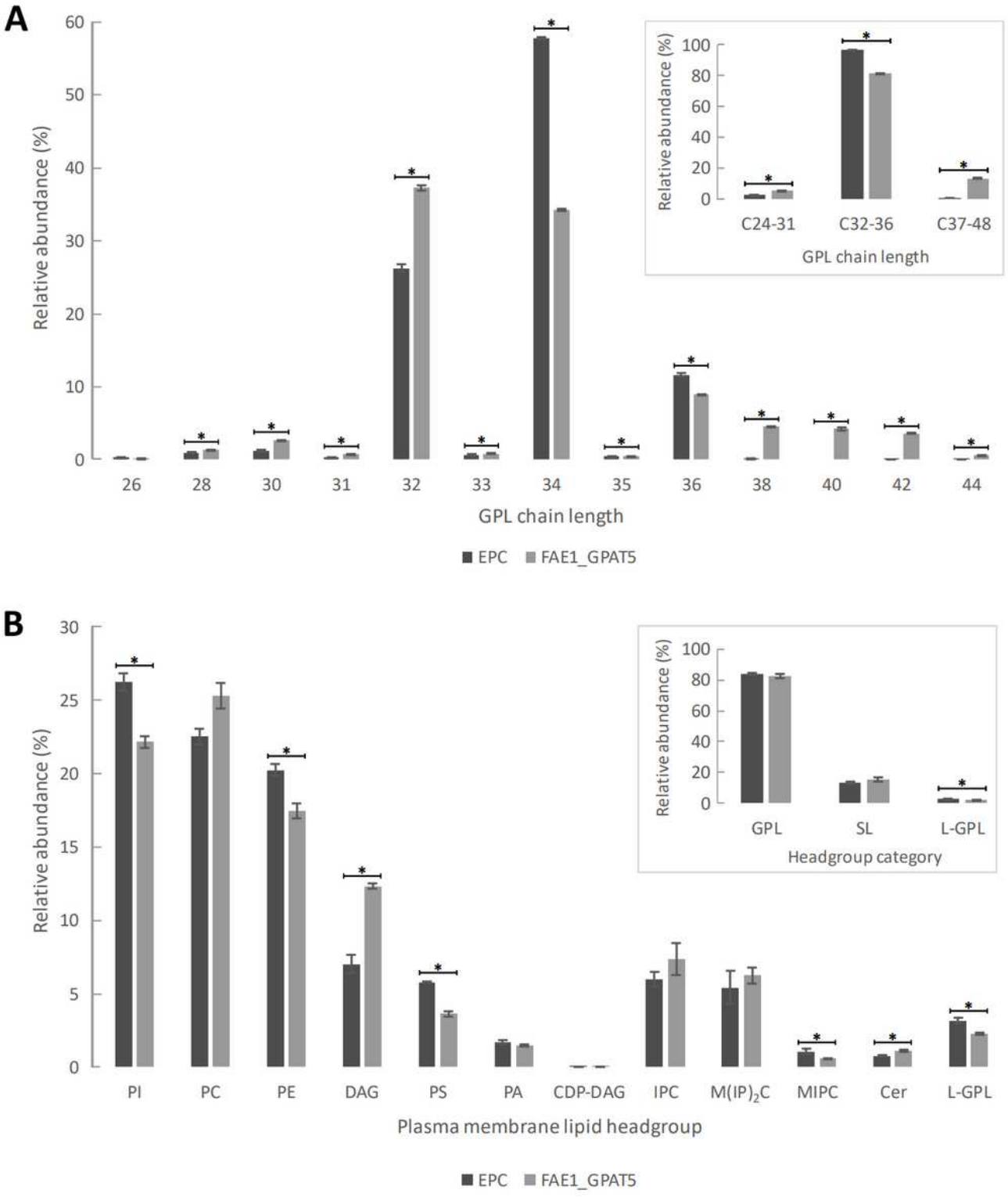

Figure 3

Glycerophospholipid acyl chain length and relative abundance of plasma membrane headgroups.

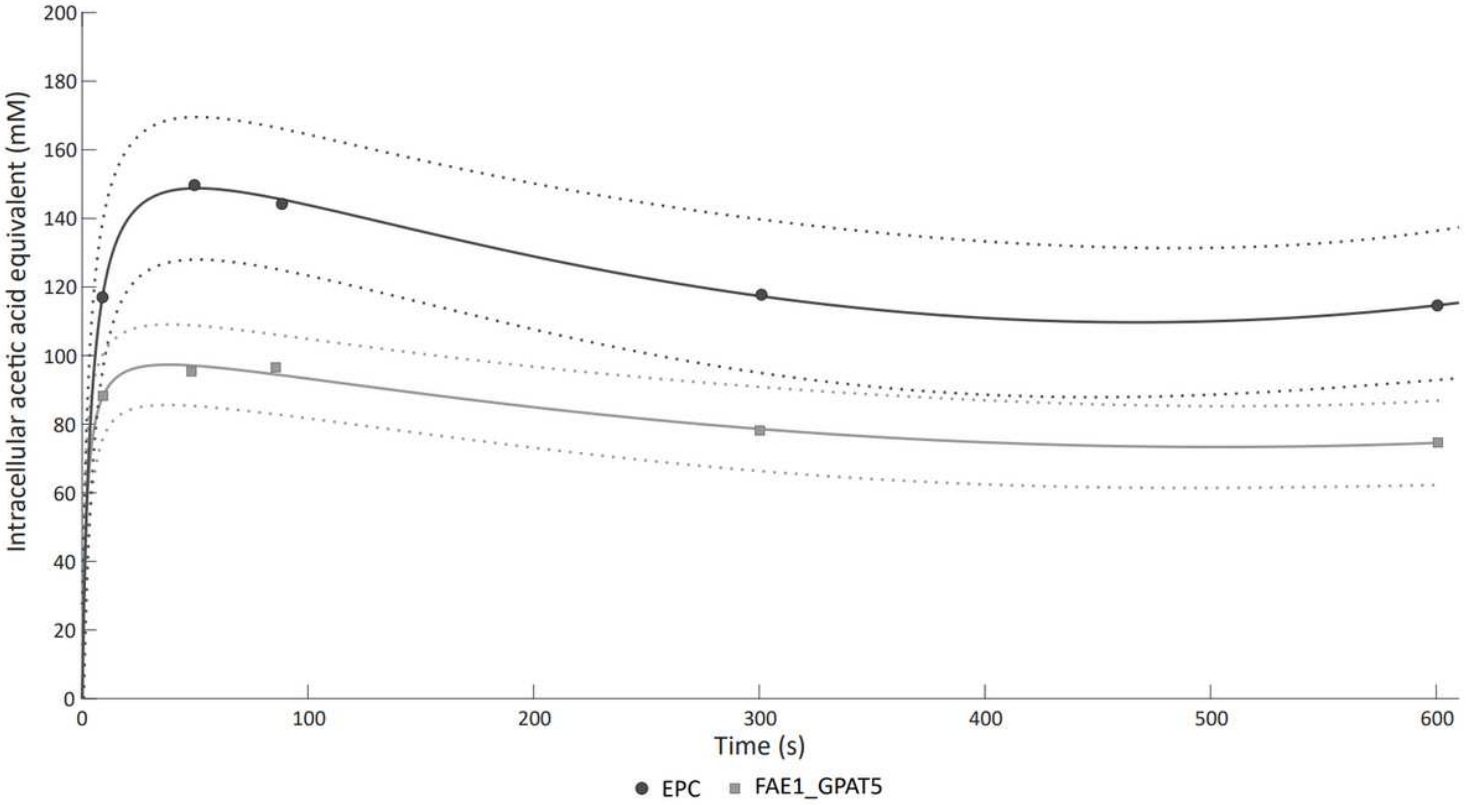

Figure 4

Acetic acid uptake with an initial extracellular acetic acid concentration of 144 mM, pH 5.0.

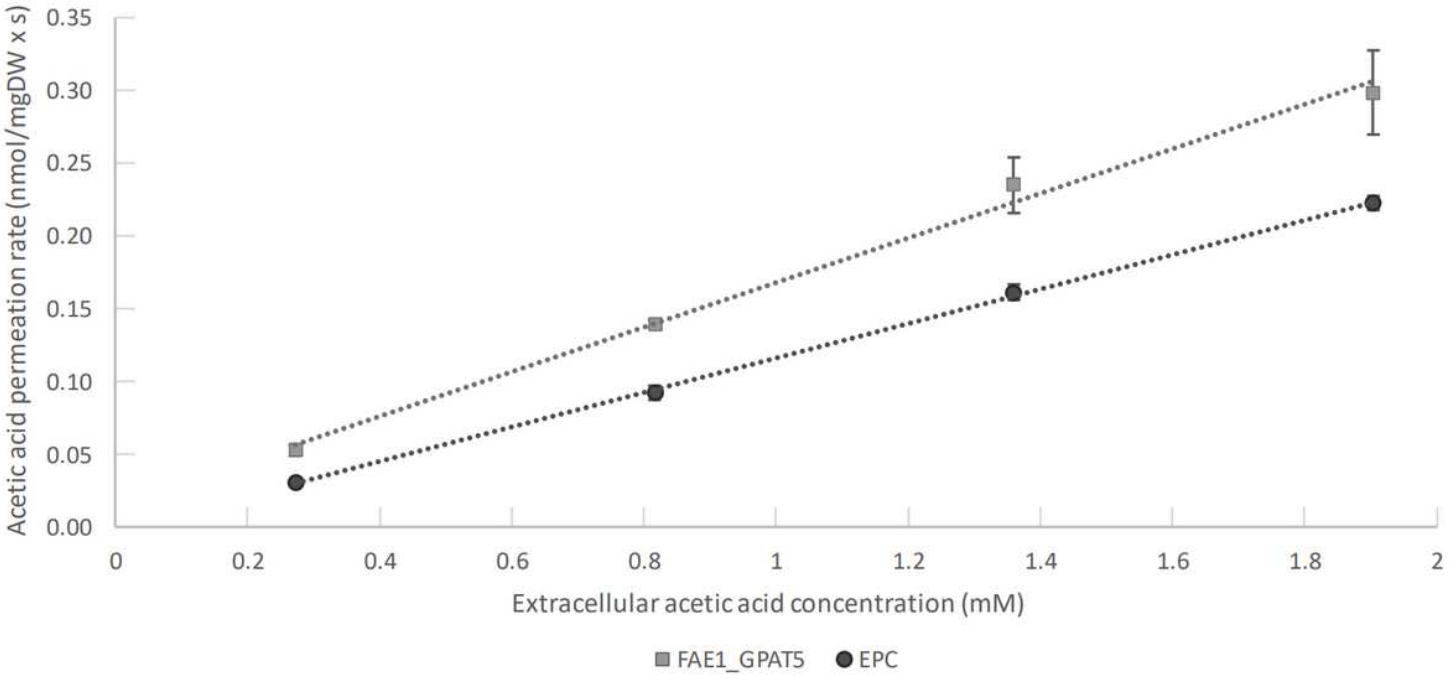

Figure 5

Acetic acid uptake kinetics.

Supplementary Files

This is a list of supplementary files associated with this preprint. Click to download.

- Illustration2Table1Maertens.pdf
- Additionalfile1Biotechnolbiofuels.docx
- Additionalfile2rawlipiddata.csv